JOURNAL OF Materials CHEMISTRY

Spin reversal and ferrimagnetism in (Gd,Ca)MnO_3

Octavio Peña,*[a] Mona Bahout,[a] Karim Ghanimi,[a] Pedro Duran,[b] Dionisio Gutierrez[b] and Carlos Moure[b]

[a]*Chimie du Solide et Inorganique Moléculaire (CSIM), UMR-CNRS 6511, Institut de Chimie de Rennes, Université de Rennes 1, 35042 Rennes Cedex, France. E-mail: pena@univ-rennes1.fr; Fax: +(33) 2.99.63.57.04; Tel: +(33) 2.23.23.67.57*

[b]*Electroceramics Department, Instituto de Cerámica y Vidrio, CSIC 28500 Arganda, Madrid, Spain*

Received 27th February 2002, Accepted 30th May 2002
First published as an Advance Article on the web 27th June 2002

The gadolinium-based manganite $GdMnO_3$, partially substituted by calcium at the cationic site, has been investigated through its crystallochemical and magnetic properties. The $Gd_{1-x}Ca_xMnO_3$ solid solution crystallises in an orthorhombic perovskite-type structure (S.G. *Pbnm*) in the range $0 \leqslant x \leqslant 0.45$. With increasing x, the structure evolves towards a quasi-tetragonal symmetry, with $c/\sqrt{2} \approx a < b$, while the orthorhombicity factor b/a decreases. The magnetisation in the ordered state was studied as a function of temperature and applied field. ZFC + FC cycles show that the solid solution can be described as a ferrimagnetic-like system, in which negatively-polarised gadolinium moments behave as free spins under the internal field of the ordered Mn sublattice. As a result, the spontaneous magnetisation changes sign upon cooling (FC process), reaching similar values as those obtained upon reversal of the magnetic field. Results are explained in terms of two interacting magnetic sublattices: a Mn-based ferromagnetic one and a negatively-aligned gadolinium network. The local field at a given site depends on the exchange interaction between these two sublattices, leading to a spin reversal when the magnetic moment of the gadolinium sublattice is larger than the ferromagnetic network. This interpretation is confirmed through the thermal evolution of the remanent magnetisation $M_{rem}(T)$ after freezing the spins using a high magnetic field.

1 Introduction

The discovery of giant magnetoresistance in doped manganese oxides of general formula $RE_{1-x}M_xMnO_3$ (where RE = rare earth, and M = divalent cation, in particular, an alkaline-earth element) has resulted in a renewed interest in these mixed-valence perovskites over the past few years.[1–3] The parent compound $LaMnO_3$ is an insulator composed of ferromagnetic planes of Mn^{3+} spins ($S = 2$) oriented in the basal plane, but antiferromagnetically coupled along the c-axis.[4] Substitution of RE by a divalent ion oxidises the MnO_3 array, creating Mn^{4+} ions ($S = 3/2$). The antiferromagnetic phase is progressively destroyed and transforms first, into a canted structure before becoming fully ferromagnetic.[4,5] The electrical and magnetic properties of these mixed-valence manganese perovskites are closely related to the ratio Mn^{3+}/Mn^{4+}, which depends on the degree of substitution of trivalent elements (RE^{3+}) by divalent cations. Other factors may also influence the magnitude and nature of the magnetic interactions, for instance, the atomic size of both the RE and dopant atoms, geometrical arguments (*i.e.*, a tolerance factor which takes into account interplane distances and bond angles[6]), the oxygen content, *etc*.

A large number of reports have described the structural, electrical and magnetic properties of pure and doped $REMnO_3$ perovksites; most of these reports concern, however, light rare-earths, that is, atoms with large ionic radii and of weak- or non-magnetic nature (*e.g.*, La, Pr, ⋯). These studies have generally been coupled with the parallel choice of large-sized dopants (*e.g.*, Sr, Ba, Pb, ⋯). Important modifications may be expected then, when small-sized elements are incorporated in the crystal structure. In addition, co-operative effects due to the intrinsic magnetism of the rare-earth network may be an important factor which may modify the magnetic response of the Mn sublattice and/or the overall magnetic behaviour of the solid solution.

More recently, reports on gadolinium-based perovskites have shown specific magnetic features, in particular a reversal of the magnetisation connected to the interplay of two interacting magnetic networks.[7,8] Similar anomalies were later found in praseodymium[9] and cerium[10] compounds, and interpreted as a ferrimagnetic ground state formed by an induced antiferromagnetic coupling of the Mn spins with the Ce spins.[11] In a parallel work, we put forward the idea that the total moment was proportional to the magnetic moment of the Mn lattice, by a factor $(1-\delta\chi_{Gd})$ which took into account the negative exchange interaction J between the Mn and Gd sublattices.[12] All these works referred to particular compounds, such as manganites $Gd_{0.67}Ca_{0.33}MnO_3$[7,12] and $Pr_{0.1}Ce_{0.4}Sr_{0.5}MnO_3$[10,11] or orthochromates $La_{0.5}Pr_{0.5}CrO_3$[9] and $GdCrO_3$.[8] However, systematic studies of the spin reversal as a function of either composition or applied experimental conditions (temperature and field) are still lacking to thoroughly describe the microscopic aspects of the magnetic interplay between both sublattices.

We have thus undertaken a full work on the mixed-valent manganite compounds (Gd,Ca)MnO_3 based on a small-sized strongly-magnetic heavy rare-earth (Gd; $\mu_{eff} = 7.96\ \mu_B$), partially substituted with a small-sized alkaline-earth element (Ca). Parallel investigations carried out on other manganites based on rare-earths of small ionic radii (*e.g.*, Y and Er) allowed us to make confident comparisons and differentiate the manganese sublattice from the intrinsic changes due to the rare-earth sublattice. We herein present the crystallochemical and magnetic properties of the $Gd_{1-x}Ca_xMnO_3$ solid solution ($0.0 \leqslant x \leqslant 0.45$), making a comparison, whenever it was of interest, with both the $Er_{1-x}Ca_xMnO_3$ and $Y_{1-x}Ca_xMnO_3$ solid solutions.

 DOI: 10.1039/b202079n

This journal is © The Royal Society of Chemistry 2002

Table 1 Lattice parameters of the solid solution $Gd_{1-x}Ca_xMnO_3$

x	$a \pm 10^{-4}$/nm	$b \pm 10^{-4}$/nm	$c \pm 10^{-4}$/nm	$c/\sqrt{2} \pm 10^{-4}$/nm	$V \pm 10^{-4}$/nm^3
0	0.5313	0.5853	0.7432	0.5255	0.2311
0.20	0.5321	0.5640	0.7473	0.5284	0.2243
0.25	0.5320	0.5580	0.7480	0.5289	0.2220
0.30	0.5326	0.5558	0.7497	0.5301	0.2219
0.35	0.5326	0.5525	0.7515	0.5314	0.2211
0.40	0.5327	0.5482	0.7528	0.5323	0.2198

2 Experimental

Reagent grade manganese oxide MnO (Merck), rare-earth oxide Gd_2O_3 (Ventron) and calcium carbonate $CaCO_3$ (Merck) powders, of submicronic particle size, were used as raw materials. Stoichiometric amounts corresponding to the $Gd_{1-x}Ca_xMnO_3$ formula ($0.0 \leqslant x \leqslant 0.45$) were weighed and homogenised by attrition milling, with isopropanol as liquid medium. The dried powders were calcined at 1000 °C for 1/2 h, attrition remilled, isostatically pressed at 200 MPa, and sintered between 1300 and 1500 °C several times. The heating rate was 2 °C min^{-1}, while cooling was performed at 1 °C min^{-1}. This thermal cycling was rigorously controlled and therefore the oxygen concentration for all samples should be identical. Besides that, and according to previous results obtained on other complex oxides (*e.g.*, superconducting materials[13]), the presence of an alkaline-earth cation (Ca^{2+}) of high electropositive character, strongly helps to maintain the oxygen stoichiometry at its theoretical limit. Apparent density was measured by water displacement; densities higher than 97% of the theoretical density were thus attained after sintering at 1350 °C for 8 hours.

Lattice parameters were determined by X-ray diffraction on a D-5000 Siemens diffractometer using CuK_α radiation and Si as an internal standard. A scanning rate of ¼° 2θ min^{-1} was used to calculate the lattice parameters (Table 1). While most of the heavy rare-earth (including Y) pure manganites $REMnO_3$ crystallise in a hexagonal symmetry (S.G. $P6_3cm$), their solid solutions of the $RE_{1-x}Ca_xMnO_3$-type show a phase transition from a biphasic region (hexagonal + orthorhombic) towards a single-phase orthorhombic region at approximately $x \sim 0.2$, depending on the rare-earth size.[14] However, in the specific case of the gadolinium-based manganite $Gd_{1-x}Ca_xMnO_3$, the solid solution over a large range of calcium substitution ($0 \leqslant x \leqslant 0.45$, *i.e.*, including the pure manganite) belongs to a single-phase region of orthorhombic perovskite-like symmetry, S.G. *Pbnm*. Table 1 shows, in particular, a smooth evolution towards a quasi-tetragonal symmetry, with $c/\sqrt{2} \approx a < b$, while the orthorhombicity factor b/a decreases when x(Ca) increases.

Magnetic properties were measured in a SHE VTS 906 SQUID magnetometer, between 5 and 400 K. The applied magnetic field ranged from 0 up to 60 kOe. In order to minimise demagnetising factors or, at least, to have similar contributions, all pieces were cut in regular shapes from ceramic disks. These pieces were then glued to a thin rod of negligible magnetic contribution; in this way, any rotation or disorientation due to torque forces was completely avoided. All measurements were performed after cooling the samples in the absence of a magnetic field. Various techniques were then applied, including: susceptibility measurements $\chi(T)$ at relatively low fields, temperature cycles (ZFC/FC) under different applied magnetic fields, magnetisation loops $M(H)$ at different constant temperatures, *etc*. In some cases, samples were cooled from room temperature down to 6 K under a high applied field of 50 kOe, the field subsequently reduced to the remanent value of the superconducting coil (*ca.* 20 Oe) and then the magnetisation $M_{rem}(T)$ recorded with increasing and decreasing temperature; in this way, the internal field due to the saturated moments (Mn sublattice) was expected to reach its maximum value before measuring the non-interacting spins contribution (Gd sublattice) in the ordered state. Additional characterisation by a.c. techniques was performed between 5 and 75 K using a home-made mutual-inductance bridge.

3 Results and discussion

3.1 Paramagnetic state

Fig. 1 shows the inverse magnetic susceptibility of some samples of the $Gd_{1-x}Ca_xMnO_3$ solid solution, measured under an applied field of 1 kOe. A paramagnetic regime is observed above $T \sim 100$ K, with fairly parallel thermal dependences for all samples, indicating an almost constant effective moment μ_{eff} and an increasing Weiss parameter θ, when x(Ca) increases. The total effective moment was evaluated from the inverse of the slope at $T \geqslant 150$ K and the Curie–Weiss temperature θ was estimated by linear extrapolation of χ^{-1}, as schematised by the linear fits in Fig. 1 (Table 2).

If we suppose that the paramagnetic regime is simply the superposition of the Mn and the RE sublattices, then their respective contributions add up in the following way:

$$C_{tot} = C(Gd) + C(Mn) \quad (3.1)$$

where $C(i)$ is the Curie constant of the i-sublattice. The magnetic moment of the manganese contribution can be evaluated from the relation:

$$\mu_{Mn} = [\mu_{eff}^2 - \mu_{Gd}^2]^{1/2} \quad (1)$$

where μ_{Gd} is the contribution of gadolinium ($\mu(Gd^{3+}) = 7.94\ \mu_B$), normalised to its concentration ($\mu_{Gd}^2 = (7.94)^2(1-x)\ \mu_B^2$). Table 2 gives the gadolinium contribution for each composition $Gd_{1-x}Ca_xMnO_3$, together with the manganese contributions calculated from eqn. [1]. It is immediately seen that a decrease of the quantity of rare-earth ion is actually compensated by the increase of the effective moment of the

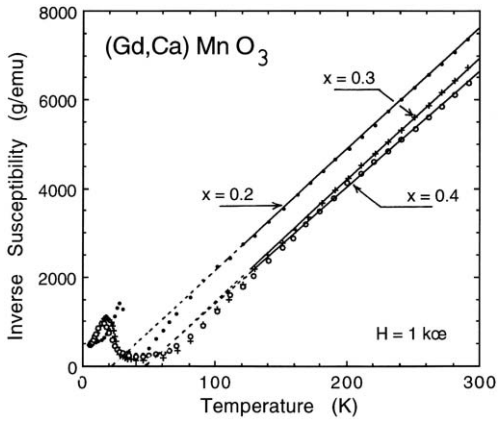

Fig. 1 Inverse magnetic susceptibility of $Gd_{1-x}Ca_xMnO_3$ measured under an applied field of 1 kOe.

Table 2 Magnetic data of the solid solution $Gd_{1-x}Ca_xMnO_3$

x(Ca)	θ/K[a]	μ_{eff} (tot)/μ_B	$\mu(Gd^{3+})/\mu_B$[b]	μ(Mn)/μ_B[c]	$T_c = T_{rev}$/K[d]
0.20	22	8.32	7.10	4.33	48
0.25	42	8.06	6.88	4.20	55
0.30	48	8.09	6.64	4.62	58
0.35	48	8.21	6.40	5.14	58
0.40	47	8.08	6.15	5.23	58

[a]Extrapolation at $\chi^{-1} = 0$ of a Curie–Weiss behaviour. [b]Assuming $\mu = 7.94\ \mu_B$/Gd-atom. [c]Magnetic contribution of the Mn sublattice, deduced from eqn. [1]. [d]Ferromagnetic ordering temperature, defined as the lowest temperature of the reversible state (see text).

Mn sublattice, leading to a more-or-less constant effective moment of the series, as a function of x(Ca).

The substitution of trivalent Gd by divalent Ca converts Mn^{3+} into Mn^{4+}. Therefore, the balance equation of the average moment gS^{av} of $Gd_{1-x}Ca_xMnO_3$ will be: $gS^{av} = (1-x)gS^{Mn^{3+}} + xgS^{Mn^{4+}}$. Considering that $S^{Mn^{3+}} = 2$ and $S^{Mn^{4+}} = 3/2$, and taking $g = 2$, then the average moment of the series should vary between 4 and 3 μ_B ($2 \geqslant S^{av} \geqslant 3/2$). In the same way, one can calculate the upper and lower limits of the effective moment μ_{eff} deduced from a Curie–Weiss law in the paramagnetic regime; in this case, μ_{eff} should vary between 4.90 μ_B and 3.87 μ_B, as $\mu_{eff}^2 = (1-x)\mu^2(Mn^{3+}) + x\mu^2(Mn^{4+})$. A glance to Table 2 shows that these values are not respected throughout the series $Gd_{1-x}Ca_xMnO_3$, being much larger than those calculated by the above equations. Even more, the effective moment increases with the conversion of Mn^{3+} into Mn^{4+}, instead of decreasing, meaning that we are in presence of magnetic clusters, and that the Mn ions are not independent entities. This result is not new and has been pointed out by other authors.[15–17]

3.2 Ordered regime

3.2.1 $\chi_{a.c.}$ and ZFC/FC cycles. Fig. 2 shows the a.c. susceptibility of the $Gd_{1-x}Ca_xMnO_3$ solid solution measured under an applied a.c. field of about 30–50 mOe, at a fixed frequency of 119 Hz. A maximum in the a.c. response is observed for all samples, ranging from 47 K up to 55 K, when x goes from 0.20 to 0.30, and slightly decreasing at higher calcium concentration (insert, Fig. 2). The peak broadens when x increases, indicating a progressive evolution of the magnetic interactions, from canted-antiferromagnetism towards ferromagnetic order, as usually observed in this kind of system.[18–20] Unfortunately, the presence of gadolinium in the samples handicaps any further investigation of the magnetic structure of these samples through neutron diffraction.

Application of a magnetic field modifies the nature of the magnetic order, according to the numerous phase diagrams

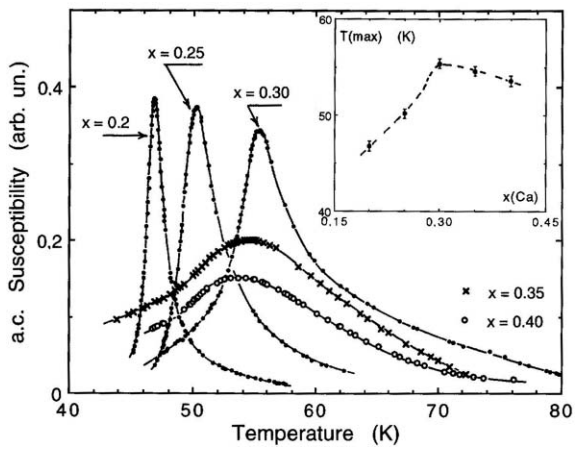

Fig. 2 a.c. susceptibility of $Gd_{1-x}Ca_xMnO_3$. Insert: T_{max} *versus* x(Ca).

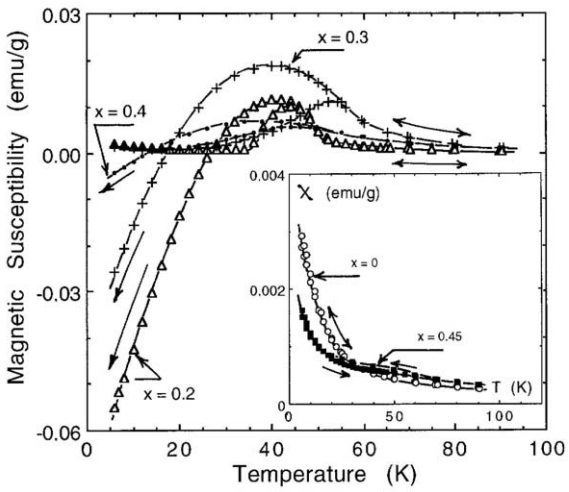

Fig. 3 ZFC/FC cycles of the solid solution $Gd_{1-x}Ca_xMnO_3$ measured under an applied field of 250 Oe.

reported in the literature.[21,22] To describe better the low-field and high-field magnetic properties, several ZFC/FC temperature cycles were performed. Fig. 3 shows the results obtained for some samples of the solid solution $Gd_{1-x}Ca_xMnO_3$, measured under an applied field of 250 Oe. For $x = 0$ and 0.45, a monotonous thermal evolution of the magnetisation is observed, while for compositions [$0.2 \leqslant x \leqslant 0.4$] a large irreversibility occurs, in which the magnetisation changes sign when cooling under the applied field. In order to investigate deeper the reversal of the magnetisation, a specific composition ($x = 0.3$, for which the amplitude of the observed phenomenon is bigger) was chosen for additional ZFC/FC experiments.

Fig. 4 shows typical results for $Gd_{0.7}Ca_{0.3}MnO_3$ under magnetic fields ranging from ~20 Oe (the remanent field of the superconducting coil) up to 15 kOe. During the warming procedure, the magnetisation first decreases, then rapidly increases up to a maximum (at T_{cusp}^{ZFC}), before reaching a reversible state (at T_{rev}). When cooling under the applied field (FC branch), the magnetisation increases up to a maximum (at T_{cusp}^{FC}), rapidly decreasing at lower temperatures: if the

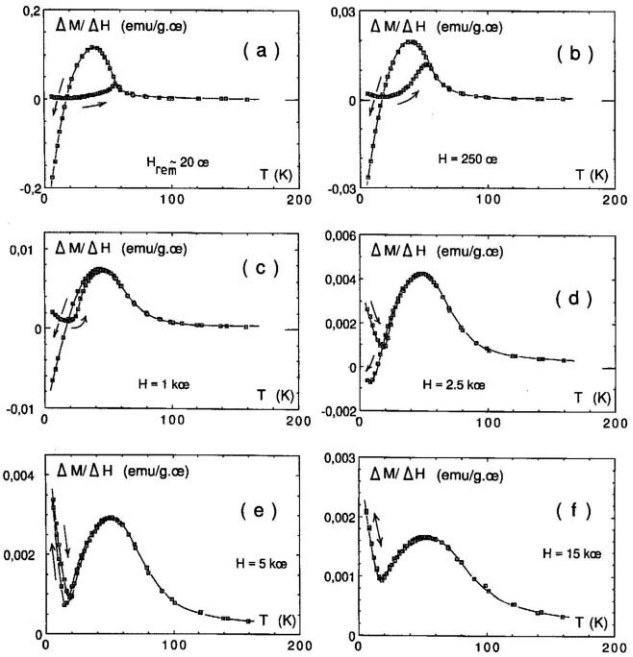

Fig. 4 Normalised magnetisation $\Delta M/\Delta H$ [emu (g Oe)$^{-1}$] of ZFC/FC cycles performed on $Gd_{0.7}Ca_{0.3}MnO_3$, and measured under given applied fields H.

magnetic field is low, the magnetisation attains negative values at the lowest temperatures (Fig. 4a, 4b and 4c) and, if the applied field is of the order of 2 kOe or more, the magnetisation increases again (Fig. 4d, 4e and 4f).

Some qualitative features are worthy of further comment:

a) an enormous hysteresis exists when H_{app} is small (Fig. 4a and 4b). In particular, two well-defined maxima are observed in the magnetisation, one at a rather fixed value $T_{cusp}^{ZFC} \sim 50$ K, the other one (at T_{cusp}^{FC}) increasing with the applied field until it reaches the same value as T_{cusp}^{ZFC},

b) two characteristic temperatures, T_{cusp}^{ZFC} and T_{rev}, are almost identical, meaning that the ferromagnetic state created while cooling (FC branch) develops from the canted-antiferromagnetism observed during the warming process (ZFC branch). This feature is quite different from that observed in other systems, where T_{cusp}^{ZFC} and T_{rev} may differ by several tens of degrees Kelvin (*e.g.*, 30 and 60 K, respectively, in $YCo_{0.25}Mn_{0.75}O_3$[23]),

c) at low temperatures, well below both maxima, a Curie–Weiss contribution can be definitely observed, as shown by the decrease of M with increasing temperature (during the ZFC branch) or the increase of M with decreasing temperature (during the FC branch). This contribution progressively increases with the external field, becoming predominant at $H_{app} \geqslant 5$ kOe,

d) in view of this description, we can say that the same phenomenon occurs for the $x = 0.45$ composition, although highly diminished since the irreversibility is only slightly observed (insert, Fig. 3).

At this point it is interesting to compare these results with those obtained in two other systems, for equivalent calcium concentrations. Fig. 5 shows the ZFC/FC cycles measured on $Y_{0.7}Ca_{0.3}MnO_3$, $Er_{0.7}Ca_{0.3}MnO_3$ and $Gd_{0.7}Ca_{0.3}MnO_3$ between 5 and 100 K, at relatively low applied fields. Three completely different behaviours can be observed, depending on the magnetic nature of the rare-earth sublattice. In the case of $Y_{0.7}Ca_{0.3}MnO_3$, the magnetisation goes through a maximum at 22 K while, with decreasing temperature, it increases just slightly below T_{cusp}^{ZFC}. We can conclude that the nonmagnetic Y ion does not contribute directly to the overall magnetic

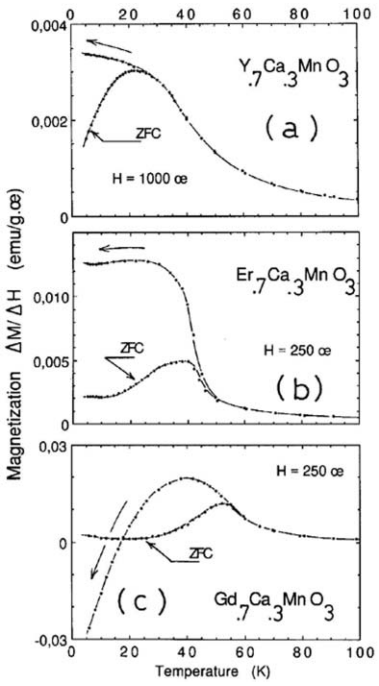

Fig. 5 Normalised magnetisation $\Delta M/\Delta H$ [emu (g Oe)$^{-1}$] of ZFC/FC cycles measured under given fields: (a) $Y_{0.7}Ca_{0.3}MnO_3$, (b) $Er_{0.7}Ca_{0.3}MnO_3$, (c) $Gd_{0.7}Ca_{0.3}MnO_3$.

behaviour, but only through the number of electrons needed to convert Mn^{3+} into Mn^{4+}. In the case of $Er_{0.7}Ca_{0.3}MnO_3$, the magnetisation reaches its maximum value at $T_{cusp}^{ZFC} \sim 39$ K while, with decreasing temperature, it raises very sharply to reach an almost constant value below ~ 30 K. It is clear that the large magnetic moment of Er ($gJ^{Er} = 9\ \mu_B$) adds up to the Mn sublattice. The most striking result comes from $Gd_{0.7}Ca_{0.3}MnO_3$, for which the magnetisation first increases with decreasing temperature, reaches a maximum at $T_{cusp}^{FC} \sim 40$ K, and then sharply decreases; at $T_{comp} = 17$ K, there is a compensation of magnetic moments ($M_{tot} = 0$), followed by negative values of the magnetisation at lower temperatures. It becomes obvious that the nature of the gadolinium ion ($gJ^{Gd} = 7\ \mu_B$) plays an important role in the overall magnetic behaviour.

3.2.2 Spin reversal. The ZFC/FC curves can be easily interpreted, as in ferrimagnetic systems, by the superposition of two interacting magnetic networks: a Mn-based ferromagnetic sublattice and a negatively-polarised gadolinium-based sublattice. On warming (after a ZFC procedure), the Mn lattice behaves as a canted-structured system, where the antiferromagnetic interplane interactions compete with the ferromagnetic in-plane exchange between Mn spins.[4] The resulting behaviour just resembles that observed in the $Y_{1-x}Ca_xMnO_3$ system, with a well-defined cusped susceptibility.[24] During this process, the gadolinium sublattice mainly experiences the effect of the external field, yielding a Curie–Weiss evolution with increasing temperature, which superposes on the Mn contribution.

On cooling under the presence of small fields ($H_{app} \leqslant 2.5$ kOe; FC procedure), the Mn lattice orders ferromagnetically, enhancing the local field at the Gd sites. If we suppose a negative exchange interaction J between the Mn and the Gd spins, then the Gd sublattice will polarise in an opposite direction to the external field. The total magnetic moment (Gd + Mn) will reach a maximum at T_{cusp}^{FC} and decrease with decreasing temperature, to become negative when $|M_{Gd}| > M_{Mn}$. In a mean-field approach, if H_{Gd} (the local field at the Gd site) is mainly due to the magnetic moment of the Mn sublattice, then

$$M_{Gd} = \chi_{Gd}(T).H_{Gd} \sim \chi_{Gd}(T).M_{Mn} \qquad (3.2.2)$$

It follows,

$$M_{tot} = M_{Gd} + M_{Mn} = -|J|.\chi_{Gd}.M_{Mn} + M_{Mn} = (1-\delta\chi_{Gd}).M_{Mn} \qquad (3.2.2)$$

where J is the negative interaction between both sublattices. It is immediately seen that, at low temperatures, when the gadolinium susceptibility ($\chi_{Gd} \sim 1/T$) becomes sufficiently large, the total moment will reverse its sign. It also follows that, the larger the applied field, the higher the contribution of the gadolinium sublattice: T_{cusp}^{FC} should move to higher temperatures, as observed.

Under the presence of high fields ($H_{app} > 5$ kOe; Fig. 4e and 4f), the situation changes slightly. The external field is larger than the internal field produced by the Mn sublattice, and it will predominate over the gadolinium susceptibility. The Gd ions remain parallel to the external field and there will be no change of the sign of the magnetisation, although a strong dip in the magnetisation is still observed at about 18 K. As pointed out in ref. 9, these curves tend to cross around $T_{comp} \sim 17$ K over the whole range of the applied fields.

Basically the same model was proposed by Snyder *et al*,[7] assuming a Mn–Gd coupling much weaker than the Mn–Mn coupling, while the Gd–Gd interaction appears to be negligible. If this is true in the present solid solution, it is no more the case in another ferrimagnetic-like manganite oxide,

$Dy_{0.7}Ca_{0.3}MnO_3$, where a similar spin reversal is observed at $T_{comp} \sim 32$ K but in which the Dy–Dy interactions persist, leading to an antiferromagnetic order at $T_N \sim 9.5$ K.[25]

3.2.3 Remanent magnetization. In order to maximise the effects of the internal field, the magnetic moment was "frozen" by cooling the sample from the paramagnetic state down to the ordered state under an applied field of 50 kOe. At 6 K, the electrical power to the superconducting coil was shut off, except for a small static remanent field (*ca.* 10–20 Oe) considered as negligible in front of the internal field created by the frozen spins. Then, a warming and cooling cycle was performed, between 6 K up to 200 K. Fig. 6 shows such measurements performed on $Gd_{0.7}Ca_{0.3}MnO_3$ and, for comparison, $Er_{0.7}Ca_{0.3}MnO_3$ (insert). Curves labelled (a) were obtained by warming the sample, starting from the "frozen state" while curves labelled (b) were recorded with decreasing temperature. Obviously, the latter are equivalent to field-cooled curves (compare to Fig. 5). It is immediately seen that erbium and gadolinium behave differently despite the fact that their free-ion moments are of the same order of magnitude ($gJ = 9$ and 7 μ_B, for Er^{3+} and Gd^{3+}, respectively).

In the $Er_{0.7}Ca_{0.3}MnO_3$ system, the erbium spins orient parallel to the internal field H_{int} produced by the Mn lattice. A Curie–Weiss contribution appears during the warming curve (a), as shown by the rapid decrease of M at low temperature; at higher temperatures, $M(T)$ slightly levels off before dropping dramatically at T_c, the ordering temperature. The erbium contribution was roughly subtracted from the total magnetic moment, obtaining the broken line (c). Comparing the variations shown by lines (c) and (b), the difference is due to the internal field due to the "freezing" procedure. We can estimate this field H_{int} by assuming a Curie law ($M = \chi.H_{int}$, where χ is the magnetic susceptibility for free Er^{3+}; $\mu_{eff}(Er^{3+}) = 9.58\ \mu_B$), yielding $H_{int} \sim 500$ Oe.

The situation differs in the $Gd_{0.7}Ca_{0.3}MnO_3$ system. The total magnetisation M, positive at 6 K, decreases rapidly with increasing temperature (curve a), becoming negative and reaching a minimum at 32 K. On further warming, M increases progressively between 32 and 58 K, changing its sign again, and becoming positive at the paramagnetic state. Such behaviour can be explained in the following way:

i) first of all, the external field applied at room temperature (50 kOe) orients the Gd ions in the same (positive) direction; on cooling from room temperature, the Gd susceptibility follows a Curie law, imposing an important local field on the Mn sublattice. Supposing a negative interaction between the Gd and Mn moments, then, at T_c and below, the Mn sublattice orients opposite to the Gd spins and freezes in a negative direction,

ii) at 6 K, once the external field has been cut off, the total internal field is the sum of two local fields: one due to the Gd sublattice, which remains oriented along the initial positive direction, and the other due to the Mn sublattice, oriented antiparallel to it,

iii) on warming (curve a), the Gd susceptibility decreases as $1/T$, while the Mn local field remains frozen in the negative direction (broken line c). As before, we can subtract the Gd contribution to estimate the internal field of the Mn sublattice, $H_{int} \sim 7000$ Oe; this value is one order of magnitude higher than the one calculated for $Er_{0.7}Ca_{0.3}MnO_3$. An internal field of about 5500 Oe due to the Cr^{3+} lattice, was also announced in the Gd orthochromate $GdCrO_3$,[8]

iv) at $T_{comp} \sim 18$ K, both contributions become of the same amplitude but with opposite sign ($M_{tot} = 0$) and, at $T >$ 32 K, the Mn moments dominate over the Gd contribution until it completely disappears at $T \geqslant T_c$,

v) on the reverse path (FC branch, curve *b*), the Mn sublattice will order first, imposing its local field to the Gd ions, which will orient antiparallel to it because of the negative exchange interaction J. On further cooling, the same process as described in section 3.2.2 takes place, the Curie–Weiss contribution of the Gd sublattice becoming predominant at low temperatures.

In other words, in $Gd_{0.7}Ca_{0.3}MnO_3$, curves (a) and (b) obey exactly the same mechanism. The only difference consists of the relative importance of the Gd and Mn internal fields: the Gd sublattice predominates when the system is cooled under an external field of 50 kOe, while the Mn sublattice imposes its direction when the system is cooled under the remanent field of 10–20 Oe.

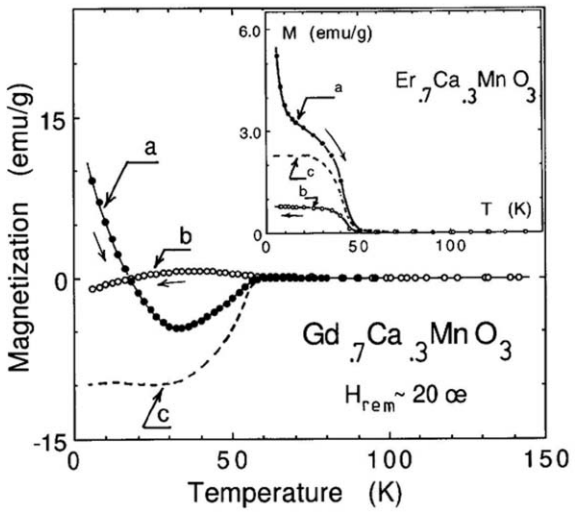

Fig. 6 Magnetisation M [emu g^{-1}] of $Gd_{0.7}Ca_{0.3}MnO_3$ and $Er_{0.7}Ca_{0.3}MnO_3$ (insert) measured under H_{rem}: (a) on warming after 50-kOe field-cooling, (b) on cooling from the paramagnetic state, (c) internal field contribution after subtracting the Curie behaviour of RE^{3+} (see text).

3.2.4 Magnetisation loops $M(H)$. Fig. 7 shows a series of magnetisation loops performed on $Gd_{0.7}Ca_{0.3}MnO_3$ at different temperatures, from 6 K up to 60 K. The maximum applied field was 60 kOe, for which a rare-earth contribution of 103 emu g^{-1} can be expected at $T = 6$ K, instead of 64 emu g^{-1} as experimentally observed. The difference should be then attributed to the antiferromagnetic polarisation of the Gd spins with respect to the Mn sublattice.

A few remarks can be made: firstly, a ferromagnetic-like $M(H)$ loop exists for temperatures up to 60 K or more. Secondly, a non-monotonical variation of the experimental slope dM/dH at low fields is clearly seen, decreasing with temperature from 6 to 20 K, then increasing between 20 and

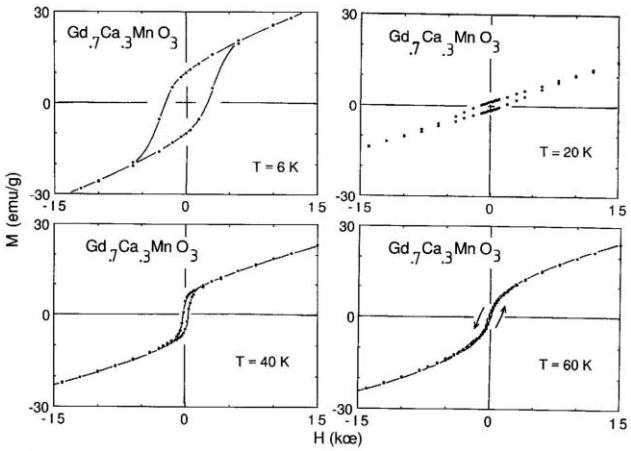

Fig. 7 Magnetisation loops $M(H)$ of $Gd_{0.7}Ca_{0.3}MnO_3$ performed at given temperatures.

40 K, and finally decreasing above 40 K. This evolution is in agreement with the thermal variation of $M(T)$ presented in Fig. 4, and thoroughly discussed in section 3.2.2. The coercive field, instead, presents a continuous and smooth change with temperature, decreasing from 2500 Oe (at 6 K) down to 0 (at $\sim$ 65 K), contrary to the non-monotonic variation in $GdCrO_3$.[8] The observed values are similar to those found in $YNi_xMn_{1-x}O_3$ and $YCo_xMn_{1-x}O_3$, specially for $x(Ni) = x(Co) = 0.33$, where a transition from canted-antiferromagnetism to a ferromagnetic state was observed.[23,26]

4 Conclusion

Useful comparisons between three rare-earth-based perovskites $(RE,Ca)MnO_3$ (RE = Y, Er and Gd) allowed us to draw important conclusions on the interplay between the magnetic contributions of both RE and Mn sublattices. The $(Y,Ca)MnO_3$ system characterises the Mn sublattice with no influence of the rare-earth magnetic moment. In $(Er,Ca)MnO_3$ the large magnetic moment of erbium superposes additively to the Mn sublattice and eventually dominates the overall behaviour of the magnetic susceptibility.

In $(Gd,Ca)MnO_3$, the Mn sublattice creates an internal field which polarises the gadolinium magnetic moments in the opposite direction, resembling the situation found in ferrimagnetic systems.[27] When cooling under small or intermediate fields ($H < 5$ kOe), the experimental magnetisation reverses its sign, reaching similar values as those obtained upon reversal of the magnetic field. Results can be interpreted in terms of two interacting magnetic networks: a Mn-based ferromagnetic sublattice and a negatively-aligned gadolinium-based sublattice. Local fields at a given site depend on the exchange (negative) interaction between these two sublattices, producing a spin reversal when the absolute value of the gadolinum network is larger than that of the ferromagnetic sublattice. Evolution of the spontaneous (remanent) magnetisation is striking as well, since this time, the Gd network imposes its direction over the Mn sublattice, also producing a similar spin reversal on warming. It is worth noting that the magnetisation reversal is also observed in a wide extent of the $Gd_{1-x}Ca_xMnO_3$ solid solution [$0.2 \leqslant x \leqslant 0.4$] and, although it has been observed for other rare-earths (*e.g.*, Ce, Pr, Dy), it does not involve all lanthanides, as we showed in the present work in the erbium case $(Er,Ca)MnO_3$.

These results prove the importance, not only of geometrical factors (size, lattice symmetry, bond distances and angles, *etc.*), but also of the magnetic nature of the different constituents in the partly-substituted manganese perovskites.

References

1 R. Von Helmolt, B. Holzapfel, L. Schulz and K. Samwer, *Phys. Rev. Lett.*, 1993, **71**, 2331.
2 K. Chahara, T. Ohno, M. Kasai and Y. Kozono, *Appl. Phys. Lett.*, 1990, **63**, 1993.
3 S. Jin, T. H. Tiefel, M. McCormack, R. A. Fastnachat, R. Ramesh and L. H. Chen, *Science*, 1994, **264**, 413.
4 E. O. Wollan and W. C. Koehler, *Phys. Rev.*, 1955, **100**, 545.
5 H. Kawano, R. Kajimoto, M. Kubota and H. Yoshizawa, *Phys. Rev. B*, 1996, **53**, 2202.
6 J. B. Goodenough, *J. Alloys Compd.*, 1997, **262–263**, 1.
7 G. J. Snyder, C. H. Booth, F. Bridges, R. Hiskes, S. DiCarolis, M. R. Beasley and T. H. Geballe, *Phys. Rev. B*, 1997, **55**, 6453.
8 K. Yoshii, *J. Solid State Chem.*, 2001, **159**, 204.
9 K. Yoshii and A. Nakamura, *J. Solid State Chem.*, 2000, **155**, 447.
10 A. Sundaresan, V. Caignaert, A. Maignan, B. Raveau and E. Suard, *Phys. Rev. B*, 1999, **60**, 533.
11 G. Martinez, J. R. Iglesias, A. R. Ruppenthal, J. M. Avignon and C. Lacroix, *J. Magn. Magn. Mater.*, 2001, **226**, 214.
12 O. Peña, *Bol. Soc. Esp. Ceram. Vidrio*, 1999, **38**, 385.
13 D. R. Clarke, T. M. Shaw and D. Dimos, *J. Am. Ceram. Soc.*, 1989, **72**, 1103.
14 C. Moure, D. Gutiérrez, J. F. Fernández, J. Tartaj, P. Durán and O. Peña, *Bol. Soc. Esp. Ceram. Vidrio*, 1999, **38**, 417.
15 C. Ritter, M. R. Ibarra, J. M. De Teresa, P. A. Algarabel, C. Marquina, J. Blasco, J. Garcia, S. Oseroff and S.-W. Cheong, *Phys. Rev. B*, 1997, **56**, 8902.
16 D. E. Cox, P. G. Radaelli, M. Marezio and S.-W. Cheong, *Phys. Rev. B*, 1998, **57**, 3305.
17 S. de Brion, F. Ciorcas, G. Chouteau, P. Lejay, P. Radaelli and C. Chaillout, *Phys. Rev. B*, 1999, **59**, 1304.
18 Y. Moritomo, A. Asamitsu and Y. Tokura, *Phys. Rev. B*, 1997, **56**, 12190.
19 M. Hennion, F. Moussa, J. Rodriguez-Carvajal, L. Pinsard and A. Revcolevschi, *Phys. Rev. B*, 1997, **56**, R497.
20 B. Dabrowski, X. Xiong, Z. Bukowski, R. Dybzinski, P. W. Klamut, J. E. Siewenie, O. Chmaissem, J. Shaffer, C. W. Kimball, J. D. Jorgensen and S. Short, *Phys. Rev. B*, 1999, **60**, 7006.
21 M. Tokunaga, N. Miura, Y. Tomioka and Y. Tokura, *Phys. Rev. B*, 1998, **57**, 5259.
22 S. Uhlenbruck, R. Teipen, R. Klingeler, B. Büchner, O. Friedt, M. Hücker, H. Kierspel, T. Niemöller, L. Pinsard, A. Revcolevschi and R. Gross, *Phys. Rev. Lett.*, 1999, **82**, 185.
23 D. Gutierrez, O. Peña, K. Ghanimi, P. Duran and C. Moure, *J. Phys. Chem. Solids*, 2002 , in press.
24 X. L. Wang, J. Horvat, H. K. Liu and S. X. Dou, *J. Magn. Magn. Mater.*, 1998, **182**, L1.
25 M. Mouallem-Bahout, O. Peña, D. Gutierrez, P. Duran and C. Moure, *Solid State Commun.*, 2002 , in press.
26 O. Peña, M. Bahout, D. Gutierrez, J. F. Fernandez, P. Duran and C. Moure, *J. Phys. Chem. Solids*, 2000, **61**, 2019.
27 A. Herpin, *Théorie du Magnétisme* Presses Universitaires de France, Paris, 1968.